

We are IntechOpen, the world's leading publisher of Open Access books Built by scientists, for scientists

4,800

Open access books available

122,000

International authors and editors

135M

Downloads

Our authors are among the

154

Countries delivered to

TOP 1%

most cited scientists

12.2%

Contributors from top 500 universities



WEB OF SCIENCE™

Selection of our books indexed in the Book Citation Index
in Web of Science™ Core Collection (BKCI)

Interested in publishing with us?
Contact book.department@intechopen.com

Numbers displayed above are based on latest data collected.
For more information visit www.intechopen.com



Investigation of the Quasi-Static and Dynamic Confined Strength of Concretes by Means of Quasi-Oedometric Compression Tests

Pascal Forquin

Abstract

For the two last decades, the quasi-oedometric compression testing method has been widely employed to characterize the quasi-static and dynamic confined response of concrete and rock-like materials. It consists of compressing a cylindrical specimen tightly enclosed in a thick confinement vessel for determining the hydrostatic and deviatoric behaviors of these materials under pressure ranging from few tens to a thousand of MPa. Large capacity hydraulic press can be used for quasi-static loading whereas large-diameter Split-Hopkinson Pressure Bar can be employed to characterize the dynamic response of the tested samples. This chapter describes the principle of this testing technique, the processing method, validation tools provided in the literature and some key-results obtained regarding the influence of concrete composition, particles reinforcement, free water content and the loading-rates on the hydrostatic and deviatoric behaviors of concretes.

Keywords: concrete, high pressure, metallic vessel, mechanical testing, quasi-oedometric compression test

1. Introduction

In many applications, geomaterials or other rock-like materials (concretes, mortars, rocks, granular materials, ice, etc.) are subjected to an intense loading characterized by high levels of pressure and high or very high rates of loading [1]. For instance, we can mention the vulnerability of concrete structures subjected to hard impact [2] in which the shear resistance and compaction law (irreversible diminution of the volume) of concrete under high pressure is known to condition the penetration of the projectile into thick targets [3–7]. One may also mention the issue of rock blasting in open quarries for the production of aggregates and sand where controlling the block size distribution is an important objective [8], the use of percussive drilling tools in civil engineering that induce high stresses beneath the indenter [9–11] or the dynamic compaction of soils. In all these applications, the geomaterial is subjected to very high confinement pressures ranging from few tens to several hundreds of MPa. A good grasp of the behavior of geomaterials under confined compression is essential to any understanding and modeling of their

performances in order to improve the efficiency of the protective solutions or the industrial applications of concern.

Triaxial tests have been developed for half a century to characterize the mechanical behavior of concretes [12] and rocks [13] under high confinement levels. It consists in applying a purely hydrostatic pressure on a cylindrical specimen by means of a fluid followed by an additional axial compression. In this case, the stress tensor is defined with the two components (σ_{radial} , σ_{axial}):

$$\bar{\sigma} = \begin{bmatrix} \sigma_{radial} & 0 & 0 \\ 0 & \sigma_{radial} & 0 \\ 0 & 0 & \sigma_{axial} \end{bmatrix} \left(\vec{U}_r, \vec{U}_\theta, \vec{U}_z \right), \quad (1)$$

where $(\vec{U}_r, \vec{U}_\theta, \vec{U}_z)$ corresponds to the frame attached to the cylindrical sample. The deviatoric stress is defined as the axial stress (in absolute value) on withdrawal of the lateral pressure exerted by the confinement fluid:

$$\sigma_{deviatoric} = |\sigma_{axial} - \sigma_{radial}|, \quad (2)$$

and the hydrostatic pressure is defined by averaging the three principle stresses:

$$P_{hydrostatic} = \frac{-\sigma_{axial} + 2\sigma_{radial}}{3} \quad (3)$$

The deviatoric strength is usually taken as the maximum deviatoric stress reached during the test and a series of triaxial tests performed at different lateral pressure provides several end-points that makes possible to deduce the limit state curves of the tested sample under static loading [14] or dynamic loading [15]. During the last decade, triaxial tests have been conducted in the 3SR laboratory with a high-capacity triaxial press (the GIGA press) able to generate a maximum confining pressure of 0.85 GPa and an axial stress of 2.3 GPa applied to cylindrical concrete specimen 7 cm in diameter and 14 cm long. As observed with quasi-oedometric compression tests [16, 17], the triaxial experiments conducted with dried, partially-saturated and fully-saturated ordinary concrete samples revealed that, under high confinement, the presence of free water in the sample affects the volumetric stiffness and reduces a lot the strength capacity [18, 19]. The role of water to cement ratio [20], cement matrix porosity [21], coarse aggregate size [22] and shape [23] in concrete samples under high triaxial compression loading was also explored with the same triaxial test apparatus. However, triaxial tests present some limitations which make them costly and difficult to perform specially under dynamic loading conditions. Indeed, they demand a very high pressure chamber (100–1000 MPa) coupled to a rigid load frame and they require impermeability between the confining fluid and the specimen that is not easy to carry out, in particular under high loading-rates. **Figure 1** provides several limit state curves obtained from triaxial tests conducted with ordinary concrete (Common concrete), high strength concrete (CRE140) and with several types of ultra-high strength (reactive powder) concretes (BPR200, BPR300, BPR 600) [24]. These experimental results illustrate the sharp increase of concrete strength as a function of the applied hydrostatic pressure. The levels of axial stress and radial stress needed to reach any points in **Figure 1** can be easily deduced considering the following equations (cf. red solid arrows and blue dotted arrows):

$$|\sigma_{axial}| = P_{hydrostatic} + \frac{2}{3}\sigma_{deviatoric}, \quad (4)$$

$$|\sigma_{radial}| = P_{hydrostatic} - \frac{1}{3}\sigma_{deviatoric}. \quad (5)$$

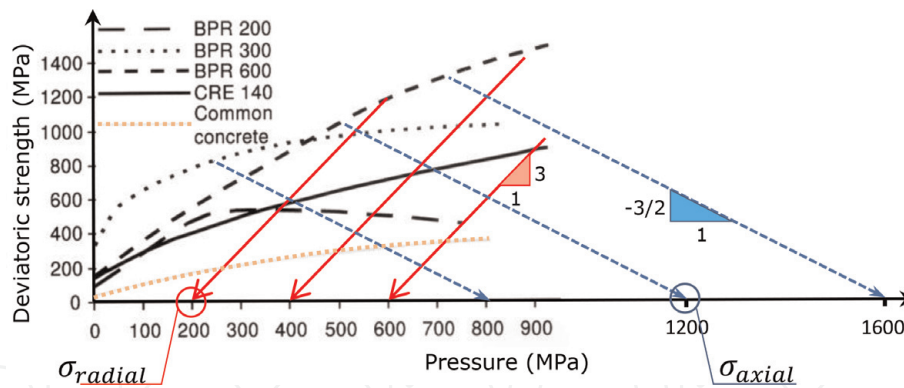


Figure 1. Limit state curves obtained from triaxial tests performed on ordinary concrete (Common concrete), high strength concrete (CRE140) and ultra-high strength concretes (BPR200, BPR300, BPR 600) [24] and corresponding levels of axial and radial stresses to be reached during the test.

Thus, it can be remarked that the last point of the “Common concrete” curve requires relatively close levels of radial stress and axial stress (respectively, about 700 and 1000 MPa) due to the small mean stress difference at this end of the test, the last point of BPR600 requires much smaller level of radial stress (about 400 MPa) and much higher level of axial stress (more than 1800 MPa). In conclusion, it appears that the level of axial and radial stresses to be applied during a triaxial or quasi-oedometric tests may need to be adapted as function of the level of the desired hydrostatic pressure and as function of the expected level of strength of the tested material.

The quasi-oedometric compression (QOC) testing method provides a very attractive alternative to triaxial tests. It is based on the use of a cylindrical sample, a confinement cell that is usually designed as a simple metallic ring, two compression plugs and an interface product that should be used to fill the gap between the sample and the inner surface of the cell. Once the sample is inserted in the confinement cell and the compression plugs are put in contact with the top and bottom surfaces of the sample, an axial compression is applied. The specimen tends to expand under the effect of its radial expansion and exerts a lateral pressure against the confinement cell. In the course of the test, a rise of both axial and radial stresses is observed in the specimen, which gives a possible reading of the mean stress difference as a function of the level of applied pressure (the so-called deviatoric behavior) and of the diminution of the sample volume with the level of hydrostatic pressure (the so-called compaction law).

A strong limitation must be underlined at that point: since the test is driven only by the axial strain, it provides a single loading path (i.e. the “quasi-oedometric loading path”) corresponding to an almost “1D” uniaxial-strain loading path. However, it cannot be concluded whether the variation of the strength is provoked mainly by the variation of the axial strain independently of the pressure level or by the change of hydrostatic pressure independently of the level of axial strain neither whether the mechanical response might be changed by subjecting the sample to a different loading path.

The QOC testing technique has been continuously developed for concretes during the last three decades. Among the proposed experimental devices, one may cite the technique developed by Bažant et al. [25] (**Figure 2(a)**) where a cylindrical concrete specimen is placed in a hole and compressed. However, the lateral pressure exerted between the sample and the inner surface of the hole could not be measured during the test. Burlion [26] devised an instrumented vessel of 53 mm as interior diameter and 140 mm as exterior diameter, which was considered stressed in its elastic domain (**Figure 2(b)**). An interface product was used between the vessel

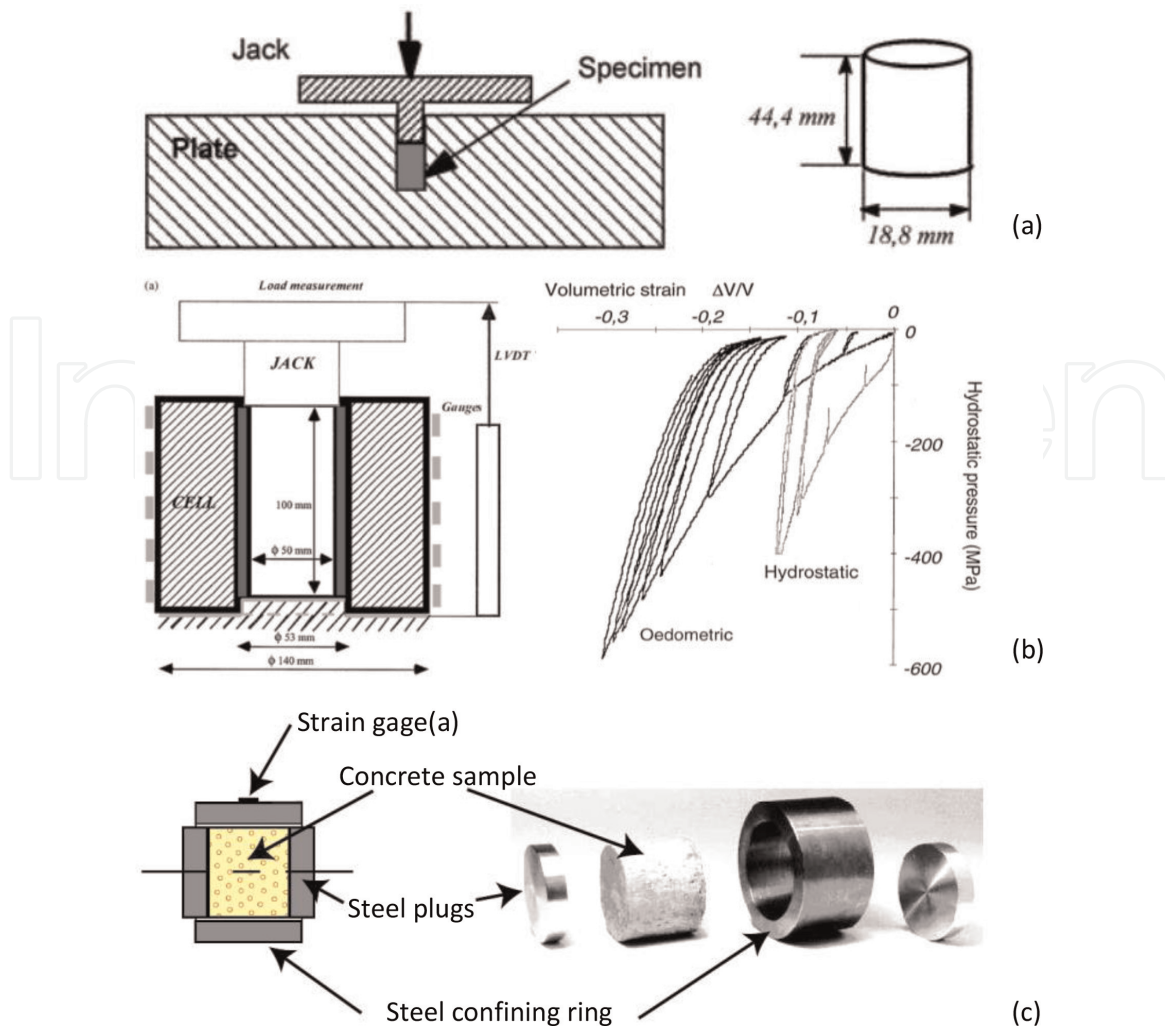


Figure 2.

Quasi-oedometric compression testing devices applied to concrete. (a) Technique method developed by Bažant et al. [25]. (b) Instrumented vessel used in [27], (c) smaller confining cells used under quasi-static and dynamic loading conditions [28].

and the specimen to fill the gap between the sample and the vessel, which allows for correcting any possible defects of cylindricity of the sample. The interface product was an epoxy bi-component resin, Chrysol® C6120, commonly used for structural applications, and once polymerized, eliminates any internal play. The radial stress in the specimen was deduced from the measurements provided by strain-gauges attached to the outer surface of the vessel [27] based on the well-known analytical solution of an elastic tube subjected to a uniform pressure applied against its whole inner surface. So, the 'barrel' deformation of the vessel was not taken into account in this analysis. Smaller confining cells, 30 or 50 mm as inner diameter and 50 or 70 mm as outer diameter, were used in [28] to test a micro-concrete under quasi-static and dynamic loadings (**Figure 2(c)**). A maximum axial strain up to -30% was reached before unloading. Later, a new processing method was proposed in [29] and applied to these experimental data to evaluate the level of radial stress in the specimen from the hoop strain measured on the outer surface of the confining cell, taking into account the sample shortening. Both deviatoric and hydrostatic responses of this microconcrete were obtained from the processed data, which showed a quite limited influence of the rate of loading on the strength, even at a strain-rate of 400 s^{-1} [30].

The testing procedure and data processing method were substantially improved in several works and applied to successively investigate the influence of particles size and shape [31, 32] and of the porosity [6] on the confined behavior of

particle-reinforced cement composites, but also to analyze the role played by free-water on the quasi-static and dynamic confined responses of microconcrete [16, 30], ordinary concrete [33] and high-performance concrete [34] and to study the effect of coarse aggregates strength on the static and dynamic behavior of concrete under high confinement [35].

In this chapter, the principle of QOC tests, the data processing technique and some validation tools are presented. Next, some main obtained results are gathered. Finally, all this data allows highlighting the main microstructural parameters influencing the mechanical behavior of concretes under quasi-static or dynamic quasi-oedometric compression loadings.

2. Principle and data processing of QOC tests

2.1 Mounting procedure

The introduction of the sample into the confining ring constitutes a very delicate stage. Indeed, to be sure that the entire gap between the sample and the inner surface of the ring is filled, it is necessary to cover the inner volume of the ring prior to inserting the sample. In addition, the sample needs to be carefully introduced without any contact with the confining cell under pain to block the sample into the ring by bow buttress. For this purpose, a special procedure was developed, as detailed in [16], to align the ring, the sample and the two plugs. First, the concrete sample is scotch tape to the upper plug. A special device (**Figure 3**) is used to introduce the concrete specimen within the ring previously partially filled by the bi-components epoxy resin named “Chryсор® C6120”. During this stage, this resin is slowly extruded out and the internal gap between the specimen and the ring is totally fulfilled by the Chryсор®, which hardens in less than 24 hours. Next, the lower and upper frames are disassembled and the assembly is ready for testing.

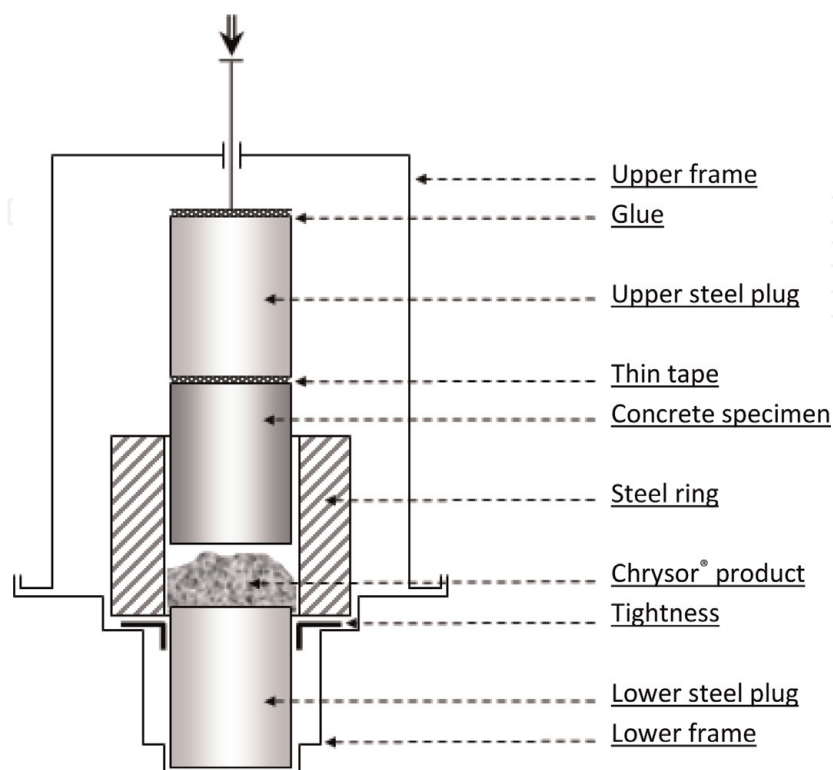


Figure 3.
Schematic of the device to set the sample, the ring and the steel plugs [16].

2.2 Description of experimental configurations

The list of concrete grades, maximum aggregate size, types of experimental set-up (hydraulic press or SHPB device), dimensions of samples and confining cells used in several works are gathered in **Table 1**. It can be remarked that the sample diameter is usually about five times larger than the maximum aggregate size. The length to diameter ratio of concrete sample is between 1 and 2. In addition, the length of the confining cell slightly exceeds the sample length in order to keep the sample inside the cell in particular when a dynamic loading is applied (SHPB device). The outer diameter is chosen as a compromise between a sufficient stiffness of the vessel (diameter large enough) and a good sensibility of strain measurements on the external surface of the vessel (small enough diameter). For this purpose, the outer diameter to inner diameter ratio varies from 1.4 [28] to 2.8 [26] with a predominance of value around 2 [6, 30–35].

Two examples of device used for quasi-static and dynamic testing are represented in **Figure 4**. The set-up represented in **Figure 4(a)** was used in [6, 31, 32] to investigate the quasi-static confined behavior of particle-reinforced cement composites. The loading capacity of the press, 1 MN, provides a maximum axial stress about 1400 MPa in the concrete sample, with a sample diameter of 30 mm. The compression plugs are fixed to the lower and upper compression plates. The extensometer that was used to measure the change of sample height is attached to two flasks directly screwed into the compression plugs. Four strain gauges are glued on the outer surface of the confining cell.

An experimental SHPB set-up, also called Kolsky's apparatus, can be used to perform dynamic QOC tests. The SHPB experimental technique, widely used today, was pioneered by Kolsky [36]. It consists in a striker, an input bar and an output bar (**Figure 4(b)**). In [16, 30, 34], the striker, the input bar and the output bar are 80 mm in diameter, their length is, respectively, 2.2, 6, and 4 m, and the elastic limit of these elements, made of high-strength steel, is 1200 MPa. When the striker hits the free end of the input bar, a compressive incident wave is generated in the input bar. Once the incident wave ($\varepsilon_i(t)$) reaches the specimen, a transmitted pulse ($\varepsilon_t(t)$) develops in the output bar whereas a reflected pulse ($\varepsilon_r(t)$) propagates in the opposite direction in the input bar. These three basic waves (cf. **Figure 4(c)**), recorded by strain gauges glued on the input and the output bars, are used to

References	Concretes [*] (Maximum aggregates size in mm)	Set-ups	Sample diameter × length	Cell outer diameter × length
[26, 27]	Mortar (2), concrete (16)	Press	D50 × 100	D140 × 106
[28, 30]	MB50 (5)	Press, SHPB	D30 × 40 D50 × 40	D50 × 50 D70 × 50
[6, 31, 32]	M1, M1M, M1Sph, M2, M2S, M2M, M2Sph (6)	Press	D30 × 40	D55 × 46
[16]	MB50 (5)	Press, SHPB	D29 × 40	D60 × 45
[34]	R30A7 (8), HSC (8)	SHPB, Press	D40 × 50	D80 × 60
[35]	R30A7, LC (10)	SHPB, Press	D40 × 50	D80 × 60

^{*}MB50: microconcrete, M1: mortar without silica fume, (M1M, M1Sph): particle-reinforced mortar without silica fume, M2: mortar with silica fume, (M2S, M2M, M2Sph): particle-reinforced mortar with silica fume, R30A7: siliceous aggregate ordinary concrete, HSC: siliceous aggregate high-strength concrete, LC: limestone aggregate ordinary concrete.

Table 1.

List of concretes, experimental set-ups, dimensions of sample and confining cell considered in several works.

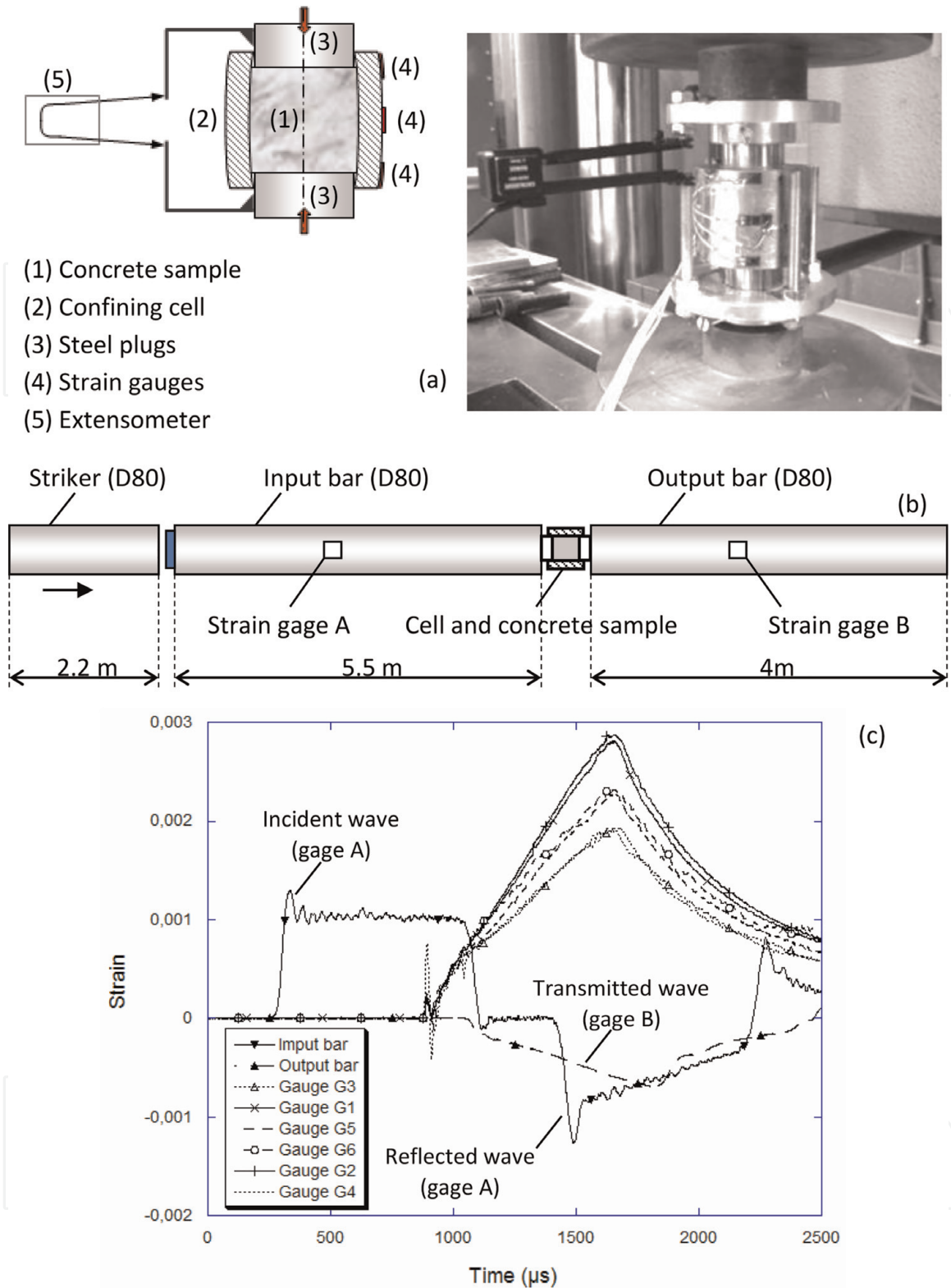


Figure 4. Experimental set-up employed for quasi-static and dynamic QOC tests. (a) Hydraulic press used in [6, 31, 32]. (b) Sketch of SHPB system used in [16, 30, 33]. (c) Example of experimental data obtained in [30].

calculate the input and output forces and the input and output velocities at the specimen faces according to the following equations (without taking into account the wave dispersion phenomena that cannot be neglected with large-diameter Hopkinson bars) [36]:

$$\begin{cases} F_{in}(t) = A_b E_b (\varepsilon_i(t) + \varepsilon_r(t)) \\ F_{out}(t) = A_b E_b (\varepsilon_t(t)) \end{cases} \quad (6)$$

$$\begin{cases} V_{in}(t) = -c_b(\varepsilon_i(t) - \varepsilon_r(t)) \\ V_{out}(t) = -c_b(\varepsilon_t(t)) \end{cases} \quad (7)$$

where A_b is the area of the input and output bars, E_b corresponds to their Young's modulus and c_b is the speed of a 1D wave propagating in these bars ($c_b = \sqrt{E_b/\rho_b}$), considering ρ_b as the density of the bars. Finally, the mean axial stress and nominal axial strain in the sample can be deduced:

$$\bar{\sigma}_{axial}(t) = \frac{F_{in}(t) + F_{out}(t)}{2A_S} \quad (8)$$

$$\bar{\varepsilon}_{axial}(t) = \int_0^t \frac{V_{out}(u) - V_{in}(u)}{h_S} du \quad (9)$$

where h_S is the sample length. In addition, the elastic limit of the plugs must be significantly higher than the maximum axial stress reached during the dynamic tests so the elastic shortening of the plugs can easily be subtracted from the total measured shortening.

2.3 Data processing of QOC tests

A processing technique was proposed in [29] to measure the radial stress in the sample taking into account the barreling deformation of the confining ring and the shortening of the concrete sample during the test. Before this approach was proposed, the closed-form solution of an elastic ring subjected to a uniform internal pressure along its whole length was usually considered but this method can lead to a strongly erroneous estimation of the radial stress in the tested sample. Later, several improvements of the processing methodology have been proposed as listed hereafter. The main advances to process the data of QOC tests are summarized in **Table 2**.

First, the relation between the radial stress in the specimen and the hoop strain measured thanks to the strain gauge glued on the outer surface of the confining cell must be deduced. The methodology used in [31] is explained in **Figure 5**. The constitutive behavior of the confining ring was first identified by means of quasi-static tensile tests performed with small samples extracted from a sacrificed ring. Next, this constitutive behavior was introduced in a numerical simulation involving only the confining vessel. Last, two calculations were conducted with the Abaqus/Standard FE code considering an internal pressure which is continuously increased up to 400 MPa, and which is applied to the inner surface of the ring along heights of 40 mm in a first

References	Advances in the processing methodology
[26, 28]	Radial stress estimated based on the close-form solution of an elastic ring subjected to a uniform internal pressure
[29]	Radial stress calculated considering the barreling deformation of the cell and the sample shortening
[31]	Radial stress calculated as in [29] and taking into the non-homogeneous and elastoplastic behavior of the cell Validation with tests applied to aluminum alloy samples
[30–32]	Estimation of the error due to friction and to the interface product by applying the processing methodology to the data of numerical simulations of QOC tests
[30, 32]	Proposition of two methods to estimate the internal friction based on strain measurements on the outer surface of the cell
[16]	Improvement of the data processing method taking into account the internal friction and the sample/cell symmetry defect based on strain measurements on the outer surface of the cell

Table 2.
Main advances proposed to process the data of QOC tests.

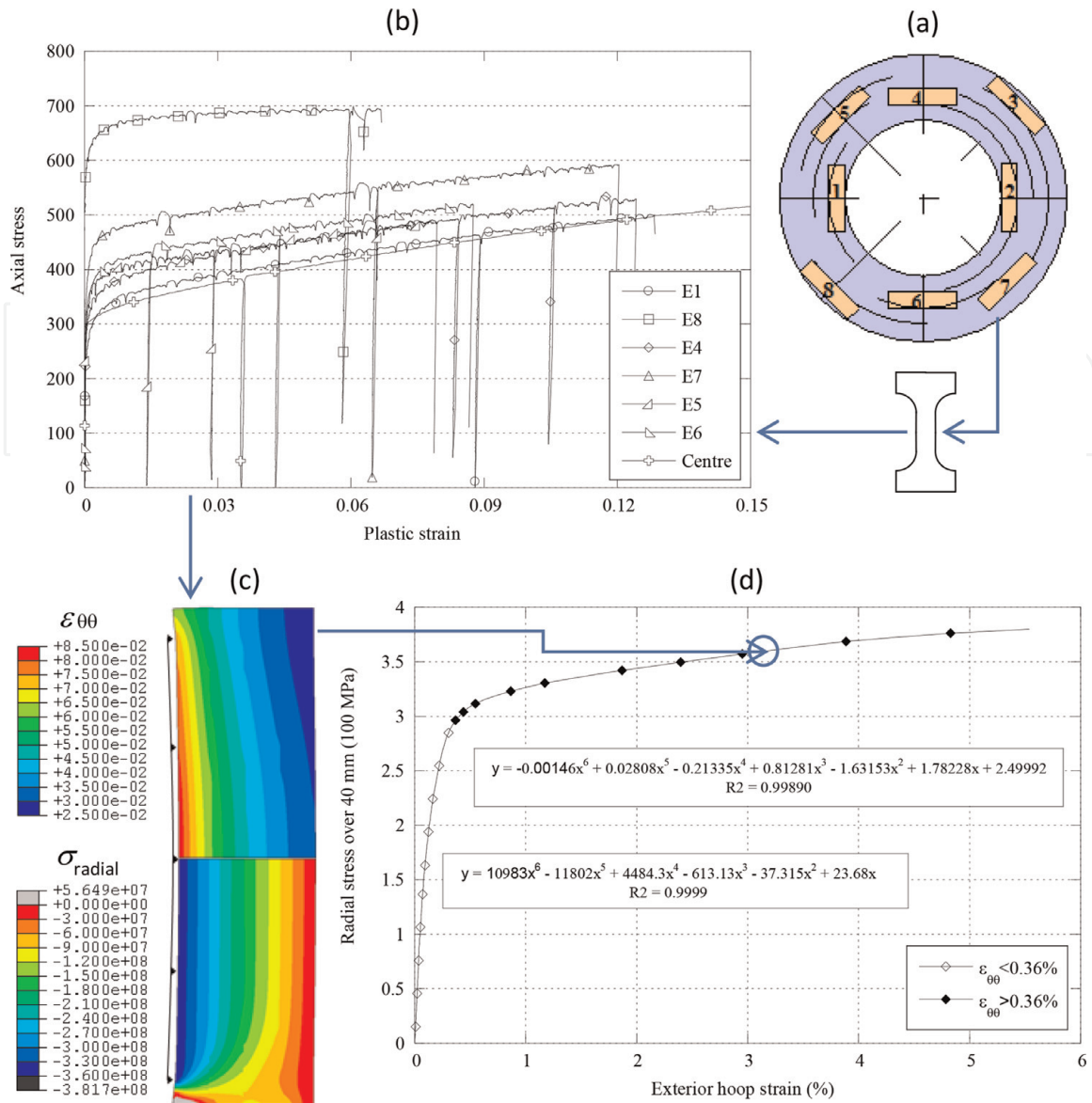


Figure 5. Methodology to determine the function $\sigma_{radial}(h=40mm) = f_{40}(\epsilon_{\theta\theta})$ [31]. (a) Extraction of small samples from a confining cell. (b) Tensile tests and identification of the elastoplastic behavior for each sample. (c) Numerical simulation of the vessel subjected to an internal pressure of 360 MPa on 40 mm (upper part: Hoop strain contours, lower part: Radial stress contours), (d) identification of the relation between the radial stress and the outer hoop strain.

calculation and 34 mm in a second calculation, these heights corresponding to the initial and final lengths of the concrete sample. From these calculations the relations: $\sigma_{radial}(h_S=40mm) = f_{40}(\epsilon_{\theta\theta}^{(z=0,ext)})$ and $\sigma_{radial}(h_S=34mm) = f_{34}(\epsilon_{\theta\theta}^{(z=0,ext)})$ were deduced, so, assuming a uniform radial stress in the sample, the radial stress was computed knowing the current height of the sample (h_S) according to the following linear interpolation:

$$\bar{\sigma}_{radial}(t) = \left(\frac{h_S(t) - 34}{40 - 34}\right) f_{40}(\epsilon_{\theta\theta}^{(z=0,ext)}) + \left(\frac{h_S(t) - 40}{34 - 40}\right) f_{34}(\epsilon_{\theta\theta}^{(z=0,ext)}) \quad (10)$$

In a similar way, the (small) radial strain in the sample was deduced based on the data of hoop strains placed at two locations on the cell ($\epsilon_{\theta\theta}^{(z=0,ext)}$, $\epsilon_{\theta\theta}^{(z=18,ext)}$):

$$\bar{\epsilon}_{radial}(t) = \frac{2}{3} \left(1 - \bar{\epsilon}_{axial} \left(1 + \frac{\bar{\epsilon}_{axial}}{2}\right)\right) \alpha_0^0 \epsilon_{\theta\theta}^{(z=0,ext)} + \frac{(1 + \bar{\epsilon}_{axial})^2}{3} \alpha_{20}^{18} \epsilon_{\theta\theta}^{(z=18,ext)} \quad (11)$$

where α_0^0 and α_{20}^{18} are coefficients identified from the same calculations.

Finally, the deviatoric stress and the hydrostatic pressure were deduced based on Eqs. (2) and (3). The volumetric strain was also calculated in the following way:

$$\bar{\varepsilon}_{volumetric}(t) = (1 + \bar{\varepsilon}_{axial})(1 + \bar{\varepsilon}_{radial})^2 - 1 \quad (12)$$

so the hydrostatic behavior of the concrete (relation between the hydrostatic pressure and the volumetric strain) was obtained. The whole procedure that was used in [6, 30–32] is summarized on the sketch of **Figure 6**.

The use of a confining cell that deforms plastically during a QOC test offers the advantage of providing higher levels of measured strains on the outer surface of the ring than with a cell that remains elastic. However, it presents several main drawbacks. First, each confining cell cannot be used more often than once due to the inelastic deformation after plasticization. Second, the relation between the radial stress in the sample and the outer hoop strain does not account for any influence of the loading rate. Therefore, if the constitutive material of the cell is strain-rate sensitive (such as steel) the relation identified under static loading is no longer valid to process the experimental data of a dynamic QOC test. Therefore, a confining cell made of brass or aluminium having a much smaller strain-rate sensitivity, can be considered [37]. Third, the plasticization of confining cell limits the maximum level of internal pressure to be applied to it. Last, the effect of friction and sample/ring dissymmetry are more difficult to calibrate in the data processing. It is the reason why, in the subsequent works, confining cell made of high strength steel ($\sigma_y > 1800$ MPa), which behavior remains elastic during the tests, were used [16, 34, 35]. In that case, the relation between the radial stress and the outer hoop strain (for a constant height of internal pressure) is linear. In the work developed in [16], a method was proposed to estimate the defect of symmetry (δ_z) represented in **Figure 7(a)**. It is based on the difference of hoop strains $\varepsilon_{\theta\theta}^{(z=+3H/8)}$ and $\varepsilon_{\theta\theta}^{(z=-3H/8)}$ measured near the top and bottom surfaces of the cell:

$$\delta_z = P_z(h) \times \left(\frac{\varepsilon_{\theta\theta}^{(z=3H/8)} - \varepsilon_{\theta\theta}^{(z=-3H/8)}}{\varepsilon_{\theta\theta}^{(z=3H/8)} + \varepsilon_{\theta\theta}^{(z=-3H/8)}} \right), \quad (13)$$

where $P_z(h)$ is a polynomial function of degree 1 valid for the considered cell. Based on a series of numerical simulations performed with different values of h and δ_z

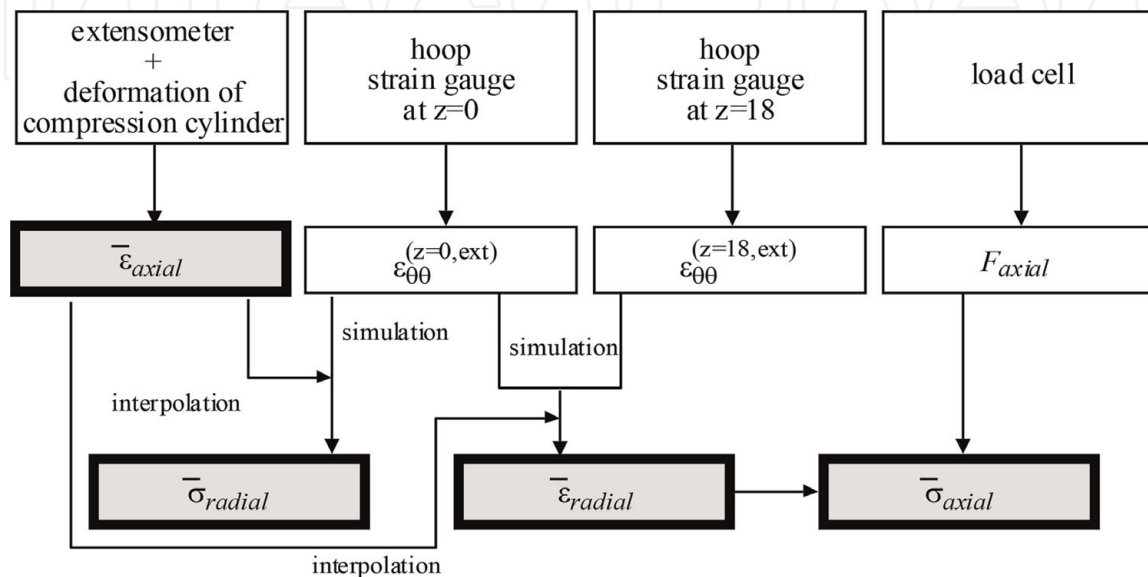


Figure 6. Procedure applied to process the data of the QOC test [31].

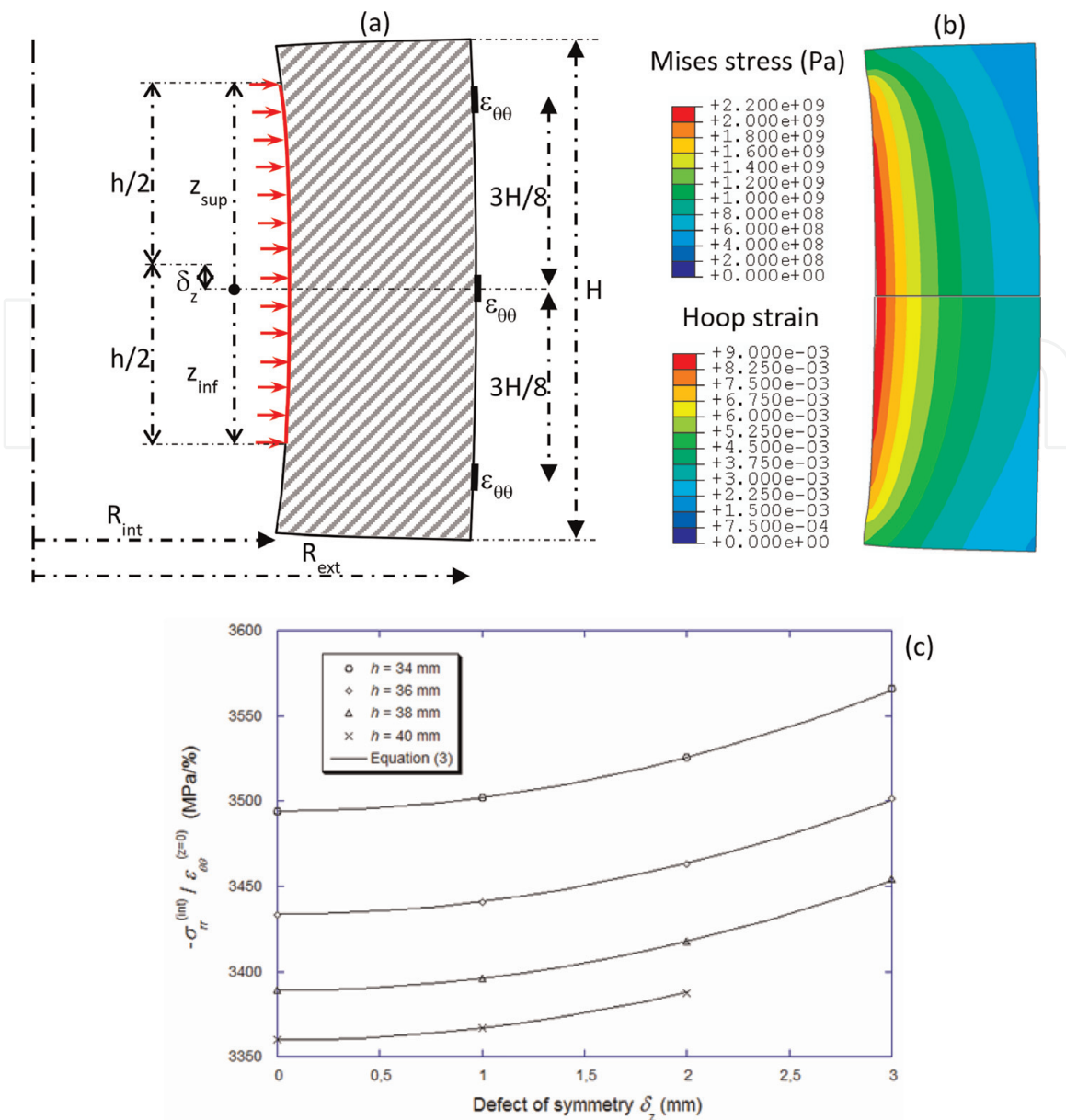


Figure 7. (a) Definition of the defect of symmetry considered in [16]. (b) Numerical simulation of an elastic cell loaded by an internal pressure of 1GPa on 40 mm (upper part: Mises stress, lower part: Hoop strain contours). (c) Radial stress to outer hoop strain ratio as function of the height of applied pressure and the defect of symmetry.

(cf. **Figure 7(b)**), the plot of **Figure 7(c)** was obtained. Finally, the ratio of radial stress to outer hoop strain can be expressed in the following way:

$$-\frac{\sigma_{radial}^{(int)}}{\epsilon_{\theta\theta}^{(z=0, ext)}} = P_{\sigma}(h) + Q_{\sigma}(h) \times (\delta_z)^2, \quad (14)$$

where $P_{\sigma}(h)$ and $Q_{\sigma}(h)$ are polynomial functions of degree 2 whose coefficients need to be identified for the considered cell. In addition, it was demonstrated in [30] that friction and the sample-cell interface was affecting the ratio of outer axial strain to the outer hoop strain at the cell middle point ($z = 0$), which provides a possible way to estimate the friction coefficient in case of a confining cell that remains elastic during the QOC test.

A validation work was developed to evaluate the accuracy and sensitivity of these processing methods to be considered for inelastic or elastic confining cells. Next, it was applied to the experimental data of QOC tests conducted with different types of concretes, mortars and high-strength concrete. The main results are summarized in the next two sections.

3. Validation of the data processing methodology

Several works have been developed to evaluate the validity and accuracy of the results obtained by applying this processing method to QOC tests. In the paper [30, 32], a series of numerical simulations of quasi-oedometric tests was conducted considering different behaviors of concrete. The Abaqus/Explicit FE code was selected to benefit from a user subroutine ‘Vumat’ in which the Krieg, Swenson and Taylor model is implemented [38, 39]. In this model, the hydrostatic behavior is described by a compaction law represented as a piece-wise linear function defined by several points (ε_v^i, p_i) (**Table 1**). On the other hand, the model includes a limitation of the equivalent stress σ_{eq} (von Mises criterion) according to the following elliptic equation that depends on the hydrostatic pressure (P)

$$(\sigma_{eq})_{limit} = \sqrt{a_0 + a_1P + a_2P^2} \quad (15)$$

The parameters used in KST model in (Forquin et al. [32]) are gathered in **Table 3**. Next, the processing methodology described in **Figure 6** was applied to the numerical data in the same way as experimental data would be processed. **Figure 8** presents the results for seven numerical simulations of a quasi-oedometric compression test. The left side of **Figure 8** corresponds to the deviatoric behavior and the right-hand column to the hydrostatic behavior. The data processing described in **Figure 6** was applied to the numerical calculations in which a friction was introduced at both plug/sample and cell/sample interfaces with a friction coefficient set to 0.1 or 0.2. Based on these numerical simulations, two methods were proposed to estimate the level of friction encountered during the QOC experiments: the first method relies on the ratio of two hoop strains measured at different locations on the outer surface of the cell. In the second method, the ratio of axial strain to hoop strain in the symmetry plane of the cell is considered. Finally it was concluded that a friction coefficient lower than 0.1 should be expected in the experiments conducted in [32]. In addition, an elastic deformation of the Chryсор® resin was simulated in two simulations with the parameters provided in **Table 3**. Finally, it was concluded that the maximum error made due to the lack of consideration of friction at plug/sample or cell/sample interfaces or Chryсор® resin in the play between the ring and the sample should not exceed about 4% regarding the deviatoric behaviour and about 12% regarding the hydrostatic behavior, whether the friction at the vessel/specimen interface remained below 0.1.

Another validation strategy was developed in [31] by conducting QOC experiments with cylindrical samples made of aluminum alloy (2017 T4), a reference material which elastoplastic behavior was well-characterized with a uniaxial tensile test. The deviatoric behavior and hydrostatic behavior obtained by data processing of one QOC test are compared with the expected responses in **Figure 9**. Again, the error made on the estimation of each deviatoric and hydrostatic response can be

Concrete (Krieg, Swenson and Taylor model)		
Elastic parameters	E, ν	46 GPa, 0.2
Compaction curve (3 points)	$\varepsilon_v^{(i)}, P^{(i)} \quad (i = 1)$	-0.0003, 7.67 MPa
	$\varepsilon_v^{(i)}, P^{(i)} \quad (i = 2)$	-0.042, 200 MPa
	$\varepsilon_v^{(i)}, P^{(i)} \quad (i = 3)$	-0.15, 580 MPa
Coefficient of elliptical equation	a_0, a_1, a_2	625 MPa ² , 270 MPa, 0.505
Chryсор® resin [31]		
Elastic parameters	E, ν	2.2 GPa, 0.28

Table 3.
Parameters used for concrete and Chryсор® resin in the calculation.

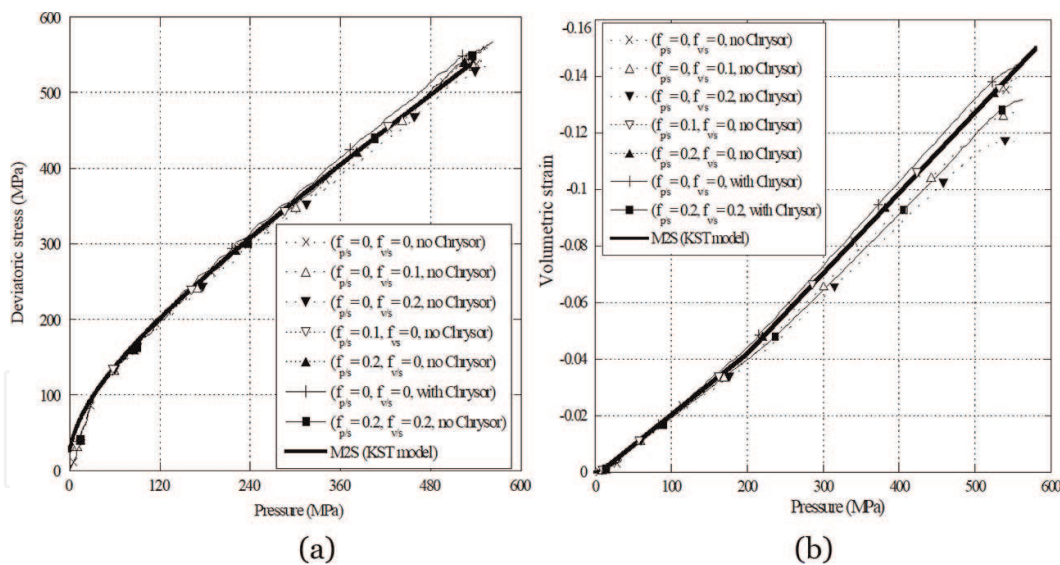


Figure 8. Processing of data from a numerical simulation of a quasi-oedometric compression test conducted with M2S small particle-reinforced mortar (cf. Table 4). (f_{ps} : Friction at plug/sample interface, f_{vs} : Friction at cell/sample interface, with Chrysol: A gap of thickness 0.3 mm is filled with a solid which behavior corresponds to a polymeric resin) [32].

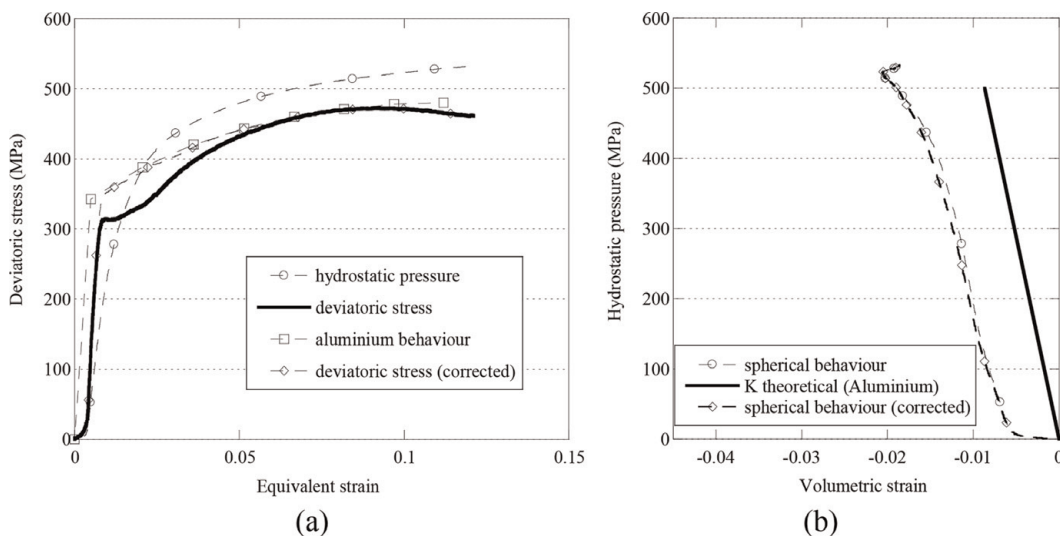


Figure 9. Quasi-oedometric compression tests applied to an aluminum alloy sample. (a) Deviatoric behavior and (b) hydrostatic behavior [31].

estimated. On the one hand, whereas the deviatoric strength is slightly underestimated in the range of weak strain it is well predicted above 5% of equivalent strain. On the other hand, the hydrostatic response shows that a gap seems to be eliminated between the compression plate and the specimen at the beginning of the test. Furthermore, the linear bulk modulus of the aluminum alloy is well captured. Finally, both validation techniques provide an estimation of error that can be made up to a certain level of pressure when applying the data processing methodology to QOC experimental data.

4. Experimental results obtained with different types of concrete

4.1 Composition of concretes tested under QOC tests

QOC experiments have been conducted and applied to different kinds of concretes, mortars, particle-reinforced mortars, microconcrete and high-strength concrete with the sample dimensions mentioned in Table 1. Their composition, the

Compositions	M1	M1M	M1Sph	M2	M2S	M2M	M2Sph
Sand (quartz) (kg/m ³)	1366	965.9		1332		941.5	
Silica fume SF (kg/m ³)	—	—		55.5		39.2	
Cement (kg/m ³)	569	402.5		555		392.3	
Water (kg/m ³)	260	183.5		253		178.9	
Admixture (kg/m ³)	4.7	3.4		4.6		3.3	
Alumina particles (kg/m ³)	0	1084.4		0		1084.4	
Shape of particles	—	Angular	Spherical	—	Angular	Spherical	
Size of particles (mm)	—	3–6	4	—	1–3	3–6	4
Water/(cement + SF)		0.46			0.41		

Table 4. Composition of mortars and particle-reinforced mortars with and without silica fume used in [6, 31, 32, 40].

Compositions	MB50	R30A7	LC	HSC
Aggregates (kg/m ³)	—	1008	891	1008
Sand (kg/m ³)	1783	838	838	795.4
Cement (kg/m ³)	400	263	263	420
Water (kg/m ³)	200	169	169	140
Silica fume SF (kg/m ³)	—	—	—	46.7
Admixture (kg/m ³)	12	—	—	4.7
Water/(cement + SF)	0.5	0.64	0.64	0.30
Max grain size (mm)	5	8	10	8

Table 5. Composition of microconcrete (MB50), siliceous aggregate ordinary concrete (R30A7) and limestone aggregate ordinary concrete (LC), siliceous aggregate high strength concrete (HSC) used in [16, 30, 34, 35].

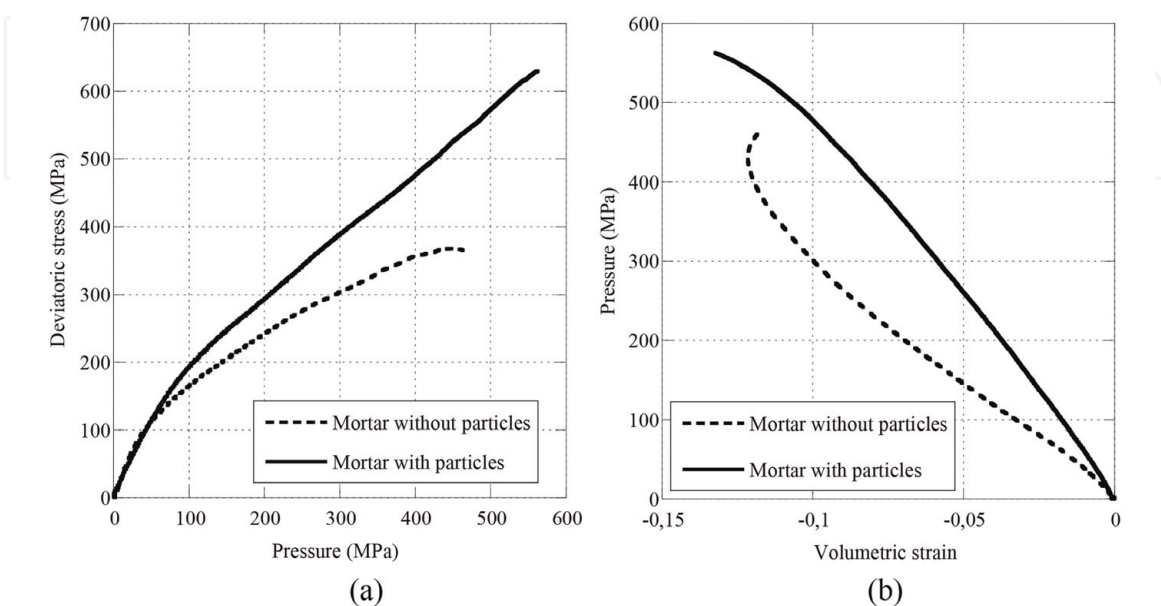


Figure 10. Quasi-oedometric compression tests applied to a mortar M2 reinforced or not with aggregates (M2M) [6]. (a) Deviatoric behavior. (b) Hydrostatic behavior.

water to cement (plus silica fume) ratio and the maximum aggregate size of the different tested materials are gathered in **Tables 4** and **5**. The most important results obtained from QOC tests are reported in the next subsections.

4.2 Influence of alumina particles used as mortars reinforcement

The benefits of alumina particles as reinforcement in two mortars were investigated in [6, 31, 32] by means of quasi-oedometric compression tests performed considering seven microstructures containing or lacking angular or spherical alumina particles. The tests showed a highly beneficial effect of the presence of particles with respect to both the deviatoric strength and the compaction law in both mortars (with and without silica fume) as illustrated in **Figure 10**, while more conventional tests (3-point bending and simple compression) did not show a such beneficial effect [40] (especially for the matrix without silica fume), proof that the strength of concretes not under confinement is not indicative of the behavior of the same materials under confined loadings. It was also found that the deviatoric strength was more favored by angular particles than by spherical ones and by the addition of silica fume in the

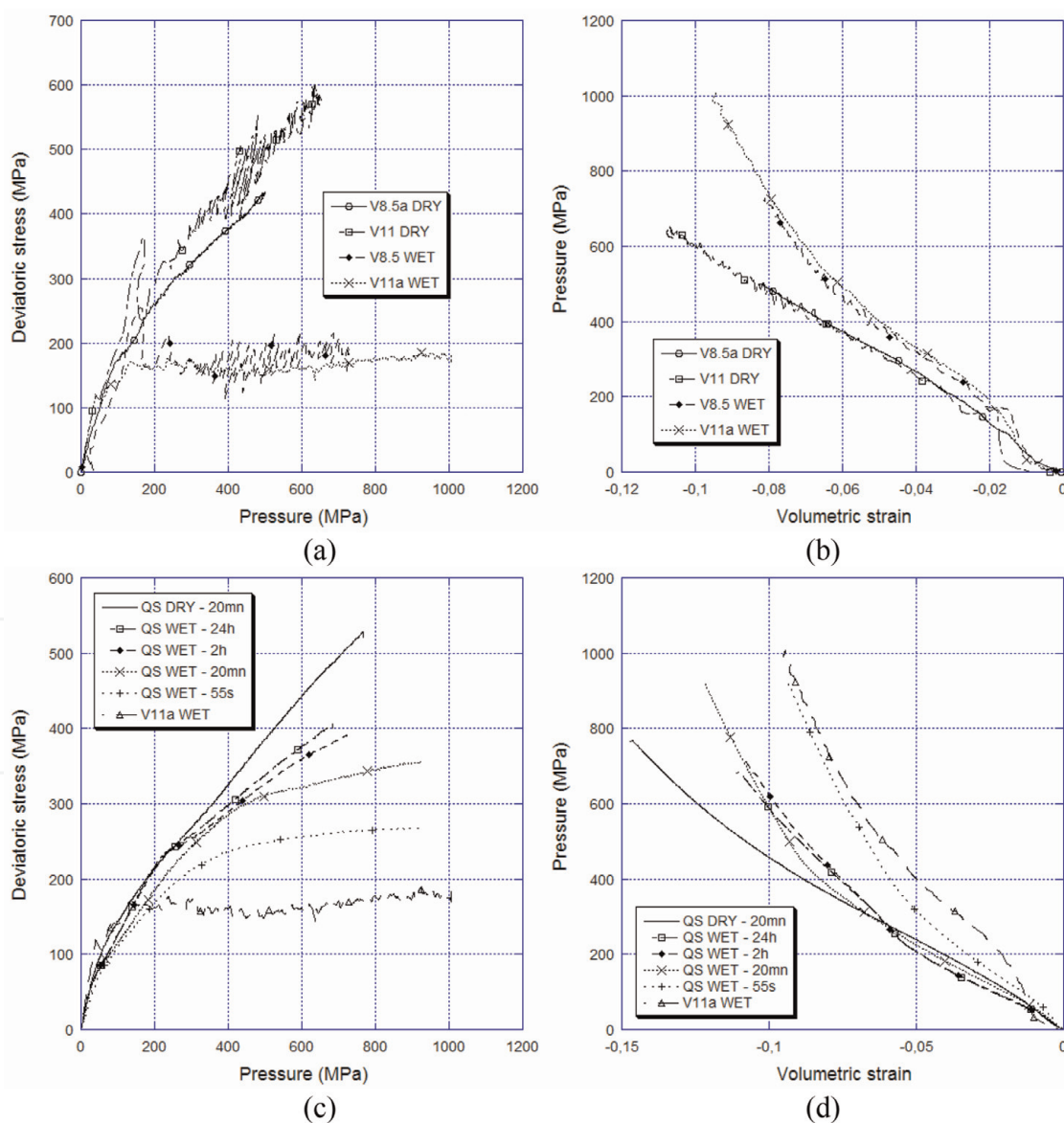


Figure 11. Quasi-oedometric compression tests applied to MB50 microconcrete [16]. (a) Deviatoric behavior and (b) hydrostatic behavior in four dynamic tests performed on dried or wet specimens. (c) Deviatoric behavior and (d) hydrostatic behavior in quasi-static and dynamic tests performed on wet specimens (V8.5 and V11 corresponding to the striking velocities equal to 8.5 m/s and 11 m/s respectively).

cement paste. In addition, a correlation was noted between the large porosities of millimeter class and the compaction of the concretes under high level of pressure. Finally, it was demonstrated that the experimental data provided by QOC experiments could be used to simulate numerically impact tests involving high levels of confining pressure in front of the projectile head [41].

4.3 Influence of free water and strain-rate on the confined behavior of microconcrete

Quasi-static and dynamic QOC tests were performed on dry and water-saturated microconcretes in [16]. The dynamic tests exhibited an important dissimilarity between dry and saturated specimens concerning both deviatoric and hydrostatic behaviors. First, dried microconcretes exhibited a continuous compaction whereas saturated specimens showed a non-linear (hardening) hydrostatic behavior (**Figure 11(b)**). Moreover, a strong and continuous increase of the strength with pressure was noted with dry samples whereas water-saturated specimens exhibited an almost-perfect saturation of the strength (**Figure 11(a)**). The quasi-static results allowed highlighting the reason of this dissimilarity (**Figure 11(c, d)**). On the one hand, dried specimens behave similarly in dynamic tests and no strain rate effect is observed. On the other hand, the behavior of saturated specimens gradually tends to that of dried specimens when the loading rate is decreased, and an expulsion of water during slow quasi-static tests was observed. Finally, it was concluded that, water-pressure inside saturated microconcrete plays a major role on their fast-quasi-static or dynamic confined behavior by reducing drastically their shear strength.

4.4 Influence of free water and strain-rate on the confined strength of ordinary concrete and high-strength concrete

The experimental results of quasi-static and dynamic QOC tests performed on dried and saturated ordinary concrete (OC, in this case, R30A7 concrete) and high-strength concrete (HSC) were compared in [34]. The main results obtained regarding their quasi-static and dynamic deviatoric responses are reported in **Figure 12**. First, under dry conditions, both OC and HSC concretes exhibit similar strength with a slightly higher strength of HSC at low pressure but with a more reduced increase of strength with pressure as compared to OC (**Figure 12(a, b)**). In addition, it can be noted that the dynamic strength of dried OC and HSC is significantly higher than their quasi-static strength whatever the considered level of pressure. Finally, the influence of strain-rate on the confined strength of dried concretes cannot be neglected.

On the other hand, under saturated conditions, both concretes exhibit completely different strength. In quasi-static conditions, a saturation of strength around 70 MPa was observed with OC, whereas the strength of HSC goes up to 270 MPa. In dynamic loading conditions, higher strengths are observed with both concretes compared with their quasi-static strengths and the influence of strain-rate cannot be neglected (**Figure 12(c, d)**). As in quasi-static loading, the dynamic confined strength of saturated HSC is much higher than that of saturated OC. Now, if dried and saturated concretes are compared, it can be concluded that the confined strength of dried samples is higher than that of saturated samples for both concretes. As concluded with microconcrete, it is supposed that interstitial water-pressure inside saturated concretes reduces their confined strength. In addition, this effect is even more pronounced in OC compared with HSC due to the higher level of porosity (11.8%) in OC as compared to HSC (8.8%), which explains the much lower

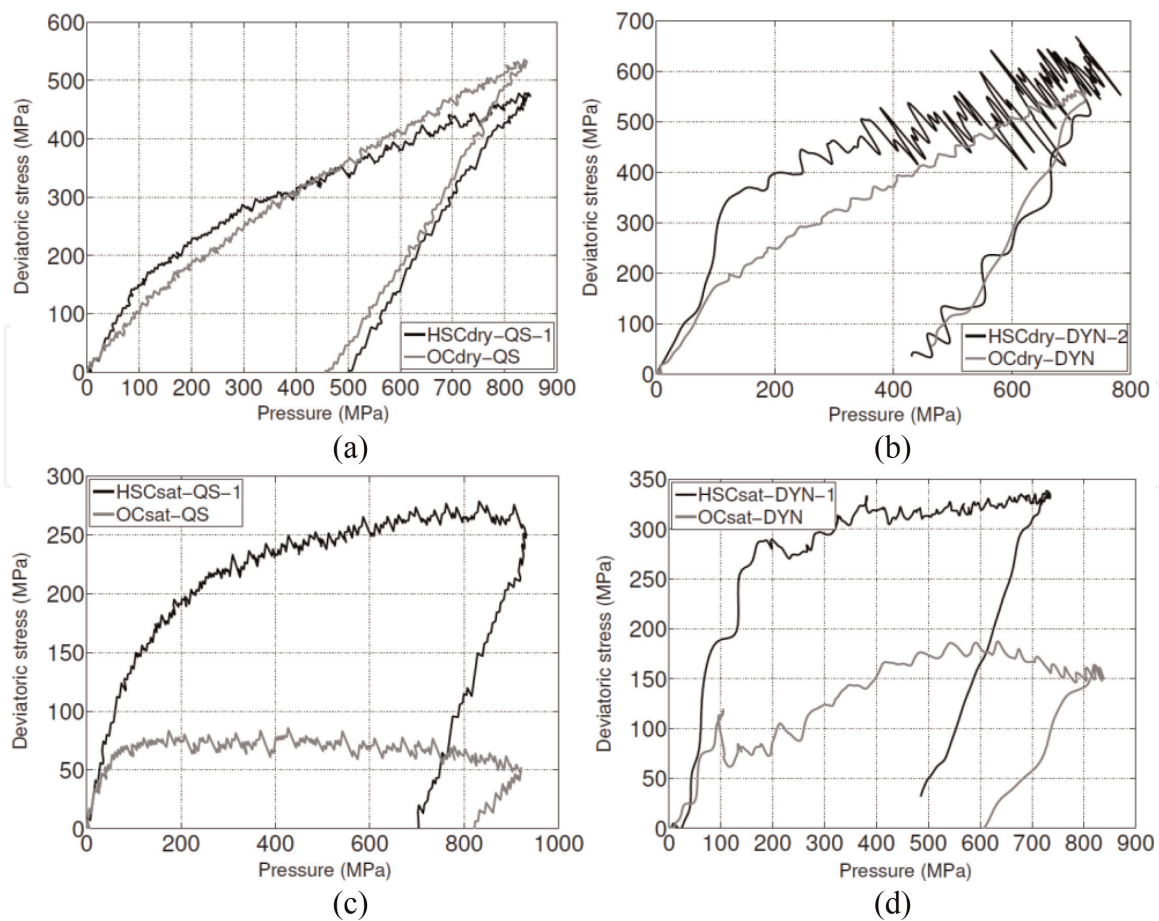


Figure 12. Quasi-oedometric compression tests applied to ordinary concrete (R30A7) and high-strength concrete in dry and saturated conditions [34]. (a) Quasi-static deviatoric behavior of dry OC and HSC concretes. (b) Dynamic deviatoric behavior of dry OC and HSC concretes. (c) Quasi-static deviatoric behavior of saturated OC and HSC concretes. (d) Dynamic deviatoric behavior of saturated OC and HSC concretes.

strength of OC in saturated condition whereas both concretes present similar strengths in dry condition.

5. Conclusion

The quasi-oedometric compression testing technique constitutes one of the most convenient and efficient testing methods to characterize the quasi-static and dynamic confined behavior of concrete and rock-like materials. However, precautionary measures need to be considered in the mounting procedure, to fill the gap between ring and the confining cell, and in the data processing to take into account for the barreling deformation of the cell, the shortening of the sample and, when necessary, for the plastic behavior of the cell, the possible effects of friction at each interface and the axial dissymmetry between the sample and the confining cell. Thus, it is possible to determine the hydrostatic and deviatoric behaviors of these materials under pressure ranging from few tens to a thousand of MPa in quasi-static loading conditions with large capacity hydraulic press or at high strain-rates with a Split-Hopkinson Pressure Bar apparatus. The main obtained results illustrate the beneficial effect of the presence of strong particles added in mortars, a strong influence of free water content on both hydrostatic and deviatoric behaviors of concretes especially in the case of microconcrete and ordinary concrete. Finally, it is concluded that concrete composition and water content have a strong influence on the concrete behavior

under high confinement and the strain-rate cannot be neglected whatever the concrete types and the water-saturation conditions.

Acknowledgements


A part of this research has been performed with the financial support of the Gramat Research Center (CEA-Gramat). The author is grateful to Dr. Eric Buzaud (CEA-Gramat) and Dr. Christophe Pontiroli (CEA-Gramat) for their sound technical and scientific advice. The quasi-static characterization in [6, 31, 32, 40] has been performed in Department of Continuum Mechanics and Structural Analysis of University Carlos III of Madrid. The author is grateful to Profs. Ramon Zaera and Angel Arias and to the Spanish Comisión Interministerial de Ciencia y Tecnología (Project MAT2002-03339), to the Comunidad Autónoma de Madrid (CCG06-UC3M/DPI-0796) and to the Délégation Générale pour l'Armement (DGA/France) for their financial support. SHPB dynamic experiments have been performed in the LMS (Laboratoire de Mécanique des Solides, Palaiseau, France). The author is grateful to Prof. Gérard Gary and Philippe Chevallier for their helpful assistance and technical support, and Prof. Patrick Le Tallec, director of the LMS, for the warm welcome.

Author details

Pascal Forquin
Laboratoire Sols Solides Structures, Risques (3SR), Université Grenoble Alpes,
CNRS, Grenoble INP (Institute of Engineering Université Grenoble Alpes),
Grenoble, France

*Address all correspondence to: pascal.forquin@3sr-grenoble.fr

IntechOpen

© 2019 The Author(s). Licensee IntechOpen. This chapter is distributed under the terms of the Creative Commons Attribution License (<http://creativecommons.org/licenses/by/3.0>), which permits unrestricted use, distribution, and reproduction in any medium, provided the original work is properly cited. 

References

- [1] Forquin P. Brittle materials at high-loading rates: An open area of research. *Philosophical Transactions of the Royal Society A*. 2017; **375**(2085):20160436. DOI: 10.1098/rsta.2016.0436
- [2] Li QM, Reid SR, Wen HM, Telford AR. Local impact effects of hard missiles on concrete targets. *International Journal of Impact Engineering*. 2005; **32**:224-284
- [3] Hanchak SJ, Forrestal MJ, Young ER, Ehrgott JQ. Perforation of concrete slabs with 48 and 140MPa unconfined compressive strength. *International Journal of Impact Engineering*. 1992; **12**(1):1-7
- [4] Xu Y, Keer LM, Luk VK. Elastic-cracked model for penetration into unreinforced concrete targets with ogival nose projectiles. *International Journal of Solids and Structures*. 1997; **34**(12):1479-1491
- [5] Yankelevsky DZ, Dancygier AN. Uniaxial Compressive Strength Effect on High Velocity Penetration into thick NSC and HSC targets. Symposium ISIEMS; 2001
- [6] Forquin P, Arias A, Zaera R. Role of porosity in controlling the mechanical and impact behaviours of cement-based materials. *International Journal of Impact Engineering*. 2008a; **35**(3): 133-146
- [7] Forquin P, Sallier L, Pontiroli C. A numerical study on the influence of free water content on the ballistic performances of plain concrete targets. *Mechanics of Materials*. 2015; **89**:176-189
- [8] Grange S, Forquin P, Mencacci S, Hild F. On the dynamic fragmentation of two limestones using edge-on impact tests. *International Journal of Impact Engineering*. 2008; **35**:977-991
- [9] Saadati M, Forquin P, Weddfelt K, Larsson P-L, Hild F. Granite rock fragmentation at percussive drilling—Experimental and numerical investigation. *International Journal for Numerical and Analytical Methods in Geomechanics*. 2014; **38**(8):828-843
- [10] Saadati M, Forquin P, Weddfelt K, Larsson P-L, Hild F. A numerical study of the influence of pre-existing cracks on granite rock fragmentation at percussive drilling. *International Journal for Numerical and Analytical Methods in Geomechanics*. 2015; **39**(5):558-570
- [11] Fourmeau M, Kane A, Hokka M. Experimental and numerical study of a drill bit drop tests on Kuru granite. *Philosophical Transactions of the Royal Society A*. 2017; **375**(2085):20160176. DOI: 10.1098/RSTA.2016.0176
- [12] Palaniswamy R, Shah SP. Fracture and stress-strain relationship of concrete under triaxial compression. *Journal of the Structural Division*. 1974; **100**:901-916
- [13] Hoek E, Franklin JA. Simple triaxial cell for field or laboratory testing of rock. *Transactions of the Institution of Mining and Metallurgy*. 1968; **77**:A22
- [14] Gabet T, Malécot Y, Daudeville L. Triaxial behaviour of concrete under high stresses: Influence of the loading path on compaction and limit states. *Cement and Concrete Research*. 2008; **38**(3):403-412
- [15] Fujikake K, Mori K, Uebayashi K, Ohno T, Mizuno J. Dynamic properties of concrete materials with high rates of tri-axial compressive loads. In: Jones N, Brebbia CA, editors. *Structures Under Shock and Impact VI*. Vol. 48. United Kingdom: WIT Press; 2000. pp. 511-522
- [16] Forquin P, Safa K, Gary G. Influence of free water on the quasi-static and

dynamic strength of concrete in confined compression tests. *Cement and Concrete Research*. 2010;**40**(2):321-333

[17] Safa K. Mise au point d'un essai de compaction dynamique. Application au béton [dissertation]. France: Ecole Polytechnique; 2008

[18] Vu XV, Malecot Y, Daudeville L, Buzaud E. Experimental analysis of concrete behaviour under high confinement: Effect of the saturation ratio. *International Journal of Solids and Structures*. 2009;**46**(5):1105-1120

[19] Malecot Y, Zingg L, Briffaut M, Baroth J. Influence of free water on concrete triaxial behavior: The effect of porosity. *Cement and Concrete Research*. 2019;**120**:207-216

[20] Vu XH, Malecot Y, Daudeville L, Buzaud E. Effect of the water/cement ratio on concrete behavior under extreme loading. *International Journal for Numerical and Analytical Methods in Geomechanics*. 2009;**33**(17):1867-1888

[21] Zingg L, Briffaut M, Baroth J, Malecot Y. Influence of cement matrix porosity on the triaxial behaviour of concrete. *Cement and Concrete Research*. 2016;**80**:52-59

[22] Vu XV, Daudeville L, Malecot Y. Effect of coarse aggregate size and cement paste volume on concrete behaviour under high triaxial compression loading. *Construction and Building Materials*. 2011;**25**(10):3941-3949

[23] Piotrowska E, Malecot Y, Ke Y. Experimental investigation of the effect of coarse aggregate shape and composition on concrete triaxial behavior. *Mechanics of Materials*. 2014;**79**:45-57

[24] Darrigade A, Buzaud E. High Performance Concrete: A Numerical

and Experimental Study 9th International Symposium on the Interactions of the Effects of Munitions with Structures. Berlin; 1999

[25] Bažant ZP, Bishop FC, Chang TP. Confined compression tests of cement paste and concrete up to 300 Ksi. *ACI Journal*. 1986;**33**:553-560

[26] Burlion N. Compaction des bétons: éléments de modélisation et caractérisation expérimentale [dissertation]. France: Ecole Normale Supérieure de Cachan; 1997

[27] Burlion N, Pijaudier-Cabot G, Dahan N. Experimental analysis of compaction of concrete and mortar. *International Journal for Numerical and Analytical Methods in Geomechanics*. 2001;**25**:1467-1486

[28] Gatuingt F. Prévion de la rupture des ouvrages en béton sollicités en dynamique rapide [dissertation]. France: Ecole Normale Supérieure de Cachan; 1999

[29] Forquin P. Endommagement et fissuration de matériaux fragiles sous impact balistique, rôle de la microstructure [dissertation]. France: Ecole Normale Supérieure de Cachan; 2003

[30] Forquin P, Gary G, Gatuingt F. A testing technique for concrete under confinement at high rates of strain. *International Journal of Impact Engineering*. 2008b;**35**(6):425-446

[31] Forquin P, Arias A, Zaera R. An experimental method of measuring the confined compression strength of geomaterials. *International Journal of Solids and Structures*. 2007;**44**(13):4291-4317

[32] Forquin P, Arias A, Zaera R. Relationship between mesostructure, mechanical behaviour and damage of cement composites under high-pressure

confinement. *Experimental Mechanics*. 2008c;**49**:613-625

Analytical Methods in Geomechanics. 1983;**7**:469-484

[33] Forquin P. Influence of free water and strain-rate on the behaviour of concrete under high confining pressure. Chapter 40. In: Song B, Casem D, Kimberley J, editors. *Dynamic Behavior of Materials, Volume 1: Proceedings of the 2014 Annual Conference on Experimental and Applied Mechanics*. The Society for Experimental Mechanics. New York: Springer; 2015. pp. 279-283

[40] Arias A, Forquin P, Zaera R, Navarro C. Relationship between bending and compressive behaviour of particle-reinforced cement composites. *Composites Part B Engineering*. 2008; **39**:1205-1215

[34] Piotrowska E, Forquin P. Experimental investigation of the confined behavior of dry and wet high-strength concrete: Quasi static versus dynamic loading. *Journal of Dynamic Behavior of Materials*. 2015;**1**(2): 191-200

[41] Forquin P, Arias A, Zaera R. An experimental method of measuring the confined compression strength of high-performance concretes to analyse their ballistic behaviour. *Journal of Physique IV*. 2006;**134**:629-634

[35] Piotrowska E, Forquin P, Malecot Y. Experimental study of static and dynamic behavior of concrete under high confinement: Effect of coarse aggregates strength. *Mechanics of Materials*. 2016;**92**:164-174

[36] Kolsky H. An investigation of mechanical properties of materials at very high rates of loading. *Proceedings of the physical society. Section B*. 1949; **62**:676-700

[37] Forquin P, Nasraoui M, Rusinek A, Siad L. Experimental study of the confined behaviour of PMMA under quasi-static and dynamic loadings. *International Journal of Impact Engineering*. 2012;**40-41**:46-57

[38] Krieg RD. A simple constitutive description for soils and crushable foams. In: SC-DR-7260883, Sandia National Laboratory. Report. USA; 1978

[39] Swenson DV, Taylor LM. A finite element model for the analysis of tailored pulse stimulation of boreholes. *International Journal for Numerical and*